

X62-71834

Copy 634

NASA TM X-10

NASA TM X-10



TECHNICAL MEMORANDUM

X - 10

DYNAMIC RESPONSE OF A SUPERSONIC DIFFUSER TO
BYPASS AND SPIKE OSCILLATION

By David N. Bowditch and Fred A. Wilcox

Lewis Research Center
Cleveland, Ohio

GPO PRICE \$

OTS PRICE(S) \$

Hard copy (HC)

Microfiche (MF)

~~DECLASSIFIED - EFFECTIVE 1-15-64~~
Authority: Memo Geo. Drobka NASA HQ.
Code ABIS-A Dtd. 3-19-64 Subj: Change
in Security Classification

NATIONAL AERONAUTICS AND SPACE ADMINISTRATION
WASHINGTON

August 1959

169-X

DECLASSIFIED

NATIONAL AERONAUTICS AND SPACE ADMINISTRATION

TECHNICAL MEMORANDUM X-10

DYNAMIC RESPONSE OF A SUPERSONIC DIFFUSER TO
BYPASS AND SPIKE OSCILLATION*

By David N. Bowditch and Fred A. Wilcox

SUMMARY

The amplitude and phase shift of static-pressure variations in a supersonic diffuser were investigated for separate oscillation of both the spike and bypass. Dynamic data are presented for the supersonic diffuser in combination with a J34 engine and three cold-pipe configurations of different length at Mach numbers of 1.8 and 2.0. Static-pressure variations were measured in the region of the terminal shock, near the bypass ports in the main duct, and near the choke point in the cold pipes. A simple method for predicting the dynamics for bypass oscillation is derived and is shown to agree reasonably well with the data.

12681

Author

INTRODUCTION

High-performance aircraft with variable-inlet features will require fast-acting closed-loop inlet controls, particularly when the inlet has internal contraction. Successful design of these controls requires a knowledge of the dynamic behavior of the supersonic inlet in combination with a turbojet engine, for which some data are presented in reference 1. These turbojet dynamics are in many respects similar to the dynamics of a supersonic inlet in combination with a ramjet engine, for which experimental data are given in reference 2. A method for the prediction of ramjet dynamics, based on separating the dynamics into a transport time and a linear system obtained from a lumped-parameter analysis, is presented in reference 3. The lumped-parameter analysis of gas-flow-system dynamics is also discussed in reference 4.

The purpose of this investigation was to determine the response of the aerodynamic portion of a closed control loop for a Mach 2.0 inlet. This dynamic response was obtained by sinusoidally oscillating the element to be controlled, in this case the bypass or spike, at frequencies up to 22 cycles per second and measuring the response of possible control pressures at locations throughout the inlet. To determine the

*Title, Unclassified.

DECLASSIFIED - EFFECTIVE 1-25-64
Authority: Memo Geo. Drobka NASA HQ.
Code ATSS-A Dtd. 3-12-64 Subj: Change
in Security Classification Marking

E-143

effect of the volume between the terminal shock and the choked exit, the inlet was equipped with a cold pipe successively choked at one of three separate stations to give a volume change of 2 to 1. Since there is a close coupling of the airflow in an engine and its inlet duct, as indicated by the results of reference 5, an inlet-engine configuration was investigated, and its dynamics were compared with those of the cold-pipe configurations.

A simple method (similar to the method of ref. 3) for predicting the response of static pressure within the inlet to bypass oscillation is derived and compared with the experimental data.

APPARATUS AND PROCEDURE

The investigation was conducted at Mach numbers of 1.8 and 2.0 at a Reynolds number of about 5.3×10^6 per foot in the 8- by 6-foot wind tunnel. A detailed description of the inlet as well as the steady-state performance of the inlet in conjunction with the J34 engine and the longest cold pipe is reported in reference 6. A schematic diagram of the engine configuration used herein is presented in figure 1(a), and the cold-pipe configurations are shown in figure 1(b). The longest cold pipe was choked by a parabolic plug, while the choke points for the short and intermediate cold pipes consisted of a plate orifice at stations 83 and 123.5, respectively, in conjunction with a movable conical plug. The area distribution of the inlet and the cold pipe is shown in figure 2.

The bypass air left the main duct in slots along the outer wall and entered an annular volume of 4.58 cubic feet (fig. 1). The bypass flow was controlled by a door in the nacelle outer skin that regulated the flow between the annular volume and the free stream. The bypass and the inlet centerbody were both hydraulically actuated and were sinusoidally oscillated at frequencies up to 22 cycles per second.

The responses of the normal shock and pressures within the inlet to the separate oscillation of the bypass and spike were measured with wall static orifices located in the region of the normal shock, at the bypass slots in the supersonic diffuser, and near the choke point (fig. 1). These static orifices were attached by short tubes to differential pressure transducers that were referenced to a constant pressure. An optical oscillograph was used to record the outputs of the pressure transducers and the bypass and spike slidewire position indicators. The phase shift and change in amplitude ratio of the measuring system from the static orifice through the recorder were negligible to 60 cycles per second.

The bypass and spike were oscillated over a series of seven or eight frequencies from 1 to 22 cycles per second. To determine the effect of various inlet conditions on the dynamics, the bypass was oscillated for combinations of spike-position parameter θ_1 of 42.6° and 45° , Mach numbers of 1.8 and 2.0, angles of attack of 0° and 6° , and bypass mean positions of 0.5 and 0.3 open. (All symbols are defined in appendix A.) The spike was oscillated for the same conditions except that the bypass was either open or closed.

The phase shift between the bypass position and the static orifices was measured peak to null and null to peak (fig. 3) because positive displacement of the bypass on the trace produced negative pressure signal movement. The value of phase shift plotted in the later figures is an average of three or four pairs of readings.

A plot of the normal-shock orifice pressure against bypass position is shown in figure 4. The plot was obtained from a trace taken while the bypass was slowly opened and closed. As can be seen in the figure, the signal is nonlinear and includes some hysteresis, at least when recorded in the preceding manner. This causes the orifice-signal amplitude ratio (amplitude divided by the amplitude at zero frequency) to be a function of bypass mean position and oscillation amplitude. Because of test conditions, the mean position and amplitude were not held constant for each series of frequencies, so that determination of the amplitude ratio became difficult. Therefore, a mean probe curve was determined (shown in fig. 4), and an equivalent bypass-oscillation amplitude was determined from the signal amplitude. The ratio of this equivalent amplitude to the actual bypass amplitude is presented as the amplitude ratio.

The normal-shock orifice signal was more linear for spike movement (not shown) than for bypass movement. Therefore, for ease of calculation, the response of the orifice was assumed to be linear, and the amplitude ratio at the lowest frequency for which there were good data was assumed to be 1.

RESULTS AND DISCUSSION

Bypass Oscillation

The dynamic data for bypass oscillation are shown in figure 5. The responses of static pressures in the normal-shock region of the long and intermediate pipes (figs. 5(a) and (d)) are very similar in general trends of amplitude ratio and phase shift. The gradual and continuous increase in phase shift with increasing frequency suggests that the system might be represented by a dead time in combination with either a first-order system or a highly damped higher order system.

The system used in this report for prediction of dynamics consists of a dead time, determined from pressure-wave travel, in series with a first-order system, where the time constant is based on the air storage capacity of the configuration. The dynamics of terminal-shock motion were calculated by the method used in reference 3. Because, however, the effects of shock dynamics were not significant for the inlet of this report at frequencies below 60 cycles per second, they were not included in the derivation. Appendix B describes the derivation of the first-order system for a cold-pipe configuration. Also included in appendix B is an extension of the system to include the engine configuration by means of correcting the volumes within the engine to diffuser-exit conditions.

The predicted phase shift fits the long and intermediate cold-pipe data quite well in the region from 1 to 10 cycles per second (figs. 5(a) and (d)). It is in this lower frequency range that the greatest difference, approximately 40° to 50° , occurs between the normal-shock-region phase-shift data of the short-pipe configuration and that of the longer cold-pipe configurations. The method of appendix B fails to predict this much difference, and therefore the predicted phase shift in the normal-shock region of the short-pipe configuration (fig. 5(e)) is about 40° higher than the average of the data. At approximately 20 cycles per second, the average phase shift in the normal-shock region for all three cold-pipe configurations is within about $\pm 10^\circ$ of the 130° phase shift. The predicted phase shifts at this frequency, consisting of the phase shift due to dead time and about 70° to 80° of phase shift from the lumped-parameter analysis, gave fair agreement for all three configurations, the prediction being approximately 30° high for the long pipe and 20° high for the other two cold-pipe configurations. At the bypass and choke-point measuring stations, the agreement of the prediction and the data follows the trends in the normal-shock region (figs. 5(b), (c), and (f)).

Above approximately 9 cycles per second, the predicted amplitude ratios are about 30 percent less than the long and intermediate test values. Because the amplitude-ratio data from the normal-shock region of the short pipe are so badly scattered, the predicted amplitude ratio is compared with the data from the region of the bypass slots (fig. 5(f)). This comparison is valid since the predicted amplitude ratio of the lumped-parameter analysis is constant throughout the configuration. The short-pipe amplitude-ratio data (best seen in fig. 5(f)) did not decrease significantly below 1 up to 22 cycles per second, while the prediction at 22 cycles per second was only 0.28.

Even though there is less volume ahead of the compressor face than there is in the small pipe, the dynamics of the engine-inlet configuration (fig. 5(g)) are very similar to those of the long pipe and are almost

identical to those of the intermediate. Therefore, the engine face cannot be considered a choke point. The engine must, then, damp the system ending at the compressor face, or its volume can be considered to be part of the system used for prediction.

The response of the inlet in combination with the engine is compared with that calculated by using diffuser-exit conditions and four different volumes. These volumes included the diffuser and bypass volume, and the engine volume obtained the following four ways: (1) calculation of an equivalent volume assuming constant ΔP throughout the engine, (2) calculation of an equivalent volume assuming constant $\Delta P/P$, (3) uncorrected engine volume, and (4) no engine volume at all. Further description of the calculation for the equivalent engine volumes and a table of the time constants for all four volumes are given in appendix B.

Comparison of these curves indicates that the phase shift of the lumped-parameter system is not very sensitive to the time constant. The time constant changes by a factor of almost 3 to 1 between the extremes of the four cases, with a corresponding maximum difference in phase shift of only 25° . The amplitude ratio, however, is more sensitive to the time constant. For the engine dynamics, the prediction based on the assumption of a constant ΔP throughout the configuration fits the data best.

In reference 1, the response of a static pressure at the normal shock in the long-pipe configuration was reported to be equal to dead time only. The obvious discrepancy between those results and present data can be attributed to two factors: the pressure sensing probe, and the fact that the reference data were for subcritical inlet operation while the present data are for supercritical operation.

The pressure sensing probe of reference 1 was a free-stream static probe projecting ahead of the cowl lip, which measured a step change in pressure when crossed by the shock. Therefore, the amplitude ratio measured by such a probe is always 1. A wall static orifice was used for the present investigation, and because of boundary-layer effects the static pressure was a continuous function of shock position. The amplitude ratio for the wall static was therefore a function of the amplitude of shock oscillation.

The second factor in the discrepancy in dynamics between reference 1 and the present report is that the response of the pressure in the diffuser and cold pipe is different for subcritical and supercritical operation. For steady-state supercritical operation, a change in bypass position results in a sizable change in diffuser-exit pressure because of a change in pressure recovery. For steady-state subcritical operation, bypass movement causes little change in pressure but effects a change in inlet mass flow. At the start of a transient, however, the diffuser

03:19:30.130
[REDACTED]

pressure in both the subcritical and supercritical cases would respond to a bypass area change at the same rate until the effect of shock movement is felt at the diffuser exit. For subcritical operation this would tend to cause the shock to overshoot after only the dead time has elapsed, and thus pass the pressure probe. Therefore, the phase shift would indicate only dead time for subcritical operation, whereas the phase shift for supercritical operation would include both dead time and diffuser lag (see appendix B).

Spike Oscillation

Reference 7 reports the characteristics of a control for the spike of this inlet that used the static pressure in the terminal-shock region. The response of that control was dependent on the diffuser dynamics for spike movement, for which data are presented in figure 6. The mass rate of air entering the inlet and the flow area at the shock position both change with spike movement and cause pressure changes throughout the configuration. Both of these changes affect the shock position directly because of local Mach number changes, and also indirectly through changes in the plenum static pressure required to match the inlet mass flow with that of the choked exit.

For spike oscillation, the phase shift in the normal-shock region increases to a maximum and then remains constant for higher frequencies. The size of the cold pipe seems to affect the frequency at which the maximum phase shift is reached but has little effect on the final value. This can be seen in figures 6(a) and (d), where a maximum phase shift of about 50° and 60° is reached at 6 and 12 cycles per second in the long and intermediate pipes, respectively. In figure 6(e), however, a phase shift of 60° is not reached in the short-pipe data until approximately 20 cycles per second (the limit of the data), so it cannot be determined whether this is a maximum. The phase shifts at the bypass and choke-point locations for the long pipe are shown in figures 6(b) and (c) and are similar to the bypass-oscillation data. This indicates that the dynamics of the volume in the diffuser and cold pipe are more predominant in this region, as might be expected.

Although there is a great deal of scatter in the amplitude-ratio data, it can be discerned that a peak occurs in the normal-shock region data (figs. 6(a), (d), and (e)) for the long and short cold-pipe configurations at about 15 cycles per second; and the amplitude ratio does not drop significantly below 1 for any of the intermediate cold-pipe configurations up to the limit of the data. This is quite different from the bypass-oscillation case where the amplitude ratio dropped to approximately 0.4 at 20 cycles per second. The amplitude ratio for the choke-point orifice for spike oscillation (fig. 6(c)) is very similar

[REDACTED]

to the bypass data up to a frequency of 9 cycles per second, above which it shows the peak or resonance exhibited in the normal-shock orifice data.

The dynamics of the engine configuration (fig. 6(f)) are again very similar to those of the intermediate-pipe configuration (fig. 6(d)). The phase shift increases to 50° at 9 cycles per second and then remains relatively constant to 18 cycles per second. The amplitude ratio also shows no tendency to drop below 1.

Probably the most important conclusion that can be made about the dynamic data for spike oscillation is that it is considerably different from the dynamics measured for bypass oscillation. It is hypothesized that this difference is due mainly to the relative location of the disturbance in the system and not to the type of disturbance. If this is the case, then the system derived in the appendix is applicable only for the case where the bypass is located well downstream of the normal-shock position in the diffuser.

SUMMARY OF RESULTS

An external-compression inlet designed for Mach 2.0 was tested in conjunction with a J34 engine and a cold pipe successively choked at three stations. The inlet centerbody and bypass were oscillated, and the response of static pressure near the terminal shock, diffuser slots for bypass air, and cold-pipe choke point was measured with the following results:

1. The phase shift of the static-pressure variations in the short, intermediate, and long cold pipes for bypass oscillation could be fairly well predicted by use of a dead time in series with a first-order lag. The predicted amplitude ratio agreed with the trends observed for all but the short-pipe configuration.

2. The response of the diffuser with the engine was almost identical to the response with the intermediate pipe for both spike and bypass oscillation. Using a corrected engine volume in the prediction method gave a curve that fit the data as well as the predictions for the long and intermediate cold-pipe configurations.

3. The spike-oscillation data were quite a bit different from the bypass-oscillation data. The phase shift of the static pressure in the normal-shock region for most configurations increased to a maximum value and remained approximately constant to the limit of the data. The short-pipe data did not conclusively show this trend because of the limited

0371300 1959
[REDACTED]

range of the data. The pipe length determined the frequency at which the maximum phase shift was reached but had only a minor effect on this maximum value.

Lewis Research Center

National Aeronautics and Space Administration
Cleveland, Ohio, February 17, 1959

APPENDIX A

SYMBOLS

A	flow area, sq ft
a	speed of sound, ft/sec
G	gain
K	constant
$L f(t)$	$\int_0^{\infty} f(t)e^{-st} dt$
M	Mach number
m	steady-state mass flow, slugs/sec
p	static pressure, lb/sq ft
R	universal gas constant, 1718 (ft-lb)/(slug)(°R)
s	Laplacian operator
T	static temperature, °R
t	time, sec
t_d	dead time, sec
V	volume of configuration, cu ft
α	angle of attack, deg
γ	ratio of specific heats
θ_z	spike-position parameter (angle between inlet centerline and line connecting spike tip and cowl lip), deg
ρ	density, slugs/cu ft
τ	time constant, sec
$\Delta()$	variation from steady-state value

03745201990

Subscripts:

- 0 stagnation conditions
- 1 inlet shock position
- 2 diffuser exit
- 3 cold-pipe exit choke point

Superscript:

- * sonic conditions

APPENDIX B

DERIVATION AND METHOD OF INLET DYNAMIC PREDICTION

The prediction of inlet dynamics is divided into two parts, as was done in reference 3 in deriving the dynamics of a ramjet engine: the dynamics of a lumped-parameter system, and a dead time based on the transport time of a pressure disturbance from the bypass to the point of pressure measurement. In the lumped-parameter system of analysis, it is assumed that the properties of the system are a function of time only, and not a function of position within the inlet. The dead time then accounts for property changes with position. For this particular analysis, it is assumed that the flow into the inlet is constant (the inlet operates supercritically) and that the volume from the terminal shock to the choked exit stores mass at a rate that is a function of diffuser-exit conditions. When analyzing the lumped-parameter system, the further simplifying assumption of combining the bypass and the plug is made, since the properties are the same throughout the system and are dependent on time only. The dead time, however, is still calculated from the bypass position. Small perturbations are assumed to allow the equations to be linearized.

Then, equating the difference in inlet and exit flows to the mass storage in perturbation form (steady-state value plus a perturbation, $m_3 + \Delta m_3$) and noting that $m_1 = m_3$ gives

$$-\Delta m_3 = \frac{d \Delta p_2 V}{dt} \quad (B1)$$

From one-dimensional isentropic flow theory, the following equation can be written for the choked exit:

$$m_3 = \frac{K_1 p_2 A_3}{\sqrt{T_2}} \quad (B2)$$

Solving for the effect of perturbations in pressure, temperature, and area from the steady-state conditions gives

$$\Delta m_3 = \frac{m_3}{p_2} \Delta p_2 - \frac{m_3}{2T_2} \Delta T_2 + \frac{m_3}{A_3} \Delta A_3 \quad (B3)$$

The equation of state and the equation for the speed of sound are combined to obtain:

$$\Delta T = \frac{\gamma - 1}{\gamma} \frac{T}{p} \Delta p \quad (B4)$$

Combining equations (B3) and (B4) gives

$$\Delta m_3 = \frac{\gamma + 1}{2\gamma} \frac{m_3}{p_2} \Delta p_2 + \frac{m_3}{A_3} \Delta A_3 \quad (B5)$$

If the volume V is assumed to be constant and the equation for the speed of sound is used, then

$$\frac{d \Delta p_2 V}{dt} = \frac{V}{\gamma R T_2} \frac{d \Delta p_2}{dt} \quad (B6)$$

Then, combining equations (B1), (B5), and (B6) and solving for Δp_2 in terms of ΔA_3 gives

$$-\frac{\gamma + 1}{2\gamma} \frac{m_3}{p_2} \Delta p_2 - \frac{V}{\gamma R T_2} \frac{d \Delta p_2}{dt} = \frac{m_3}{A_3} \Delta A_3 \quad (B7)$$

By taking the Laplace transforms and rearranging terms, the following equation is obtained:

$$\frac{\Delta p_2(s)}{\Delta A_3(s)} = - \frac{\frac{2\gamma}{(\gamma + 1)} \frac{p_2}{A_3}}{1 + \frac{2p_2 V}{(\gamma + 1)m_3 R T_2} s} \quad (B8)$$

Equation (B8) is for a first-order system where the gain and time constants are

$$G = - \frac{2\gamma}{\gamma + 1} \frac{p_2}{A_3} \quad (B9)$$

and

$$\tau = \frac{2p_2 V}{(\gamma + 1)m_3 R T_2} = \frac{2}{(\gamma + 1)} \frac{V}{\frac{\rho^*}{\rho_2} a^* A_3}$$

The Laplace transformation for a time function including dead time is

$$L \Delta P(t - t_d) = e^{-t_d s} \Delta p(s)$$

Combining the dead time and the lumped-parameter transformations gives

$$\frac{\Delta p_2(s)}{\Delta A_3(s)} = \frac{Ge^{-t_d s}}{1 + \tau s}$$

In the following table the time constants and dead times are presented for the inlet operating critically at Mach 1.8 with the spike positioned at $\theta_1 = 45^\circ$. The cold-pipe-configuration time constants were determined by using the diffuser-exit conditions and the sum of the volumes of the diffuser, bypass, and cold pipe. For the engine configuration, four time constants were calculated by using the diffuser-exit conditions, the sum of the diffuser and bypass volumes, and the engine volume treated by four different methods. Two of the methods used attempted to correct the engine volume to an equivalent volume at diffuser-exit conditions having an equal storage capacity. The assumptions used for these two methods were that Δp was constant throughout the engine, making the correction factor $(\Delta p / \Delta p_2)$ inversely proportional to the local temperature, and that $\Delta p / p$ was constant, in which case the correction factor is proportional to the ratio of the local density to the station 2 density. The third and fourth time constants were calculated for comparison and used both the uncorrected engine volume and no engine volume at all.

Lumped-parameter time constants

[Diffuser volume, 8.41 cu ft; bypass volume, 4.58 cu ft;
 $T_0 = 584^\circ \text{R}$; $M_2 = 0.30$; $A_3 = 1.175 \text{ sq ft.}$]

Configuration	Cold-pipe or engine volume, cu ft	Config- uration volume, V, cu ft	Time constant, τ , sec
Long cold pipe	21.49	38.48	0.0341
Intermediate cold pipe	13.99	26.98	.0267
Short cold pipe	4.07	17.06	.0169
Engine	14.69	27.68	.0274
Engine, $\Delta p = \text{constant}$	8.86	21.85	.0216
Engine, $\Delta p / p = \text{constant}$	21.77	34.76	.0344
Diffuser and bypass	0.00	12.99	0.0129

03:19:30.1030

The dead time was calculated by graphically integrating a plot of the reciprocal of the vector sum of the pressure-wave velocity and the stream velocity against position in the inlet. The wave is assumed to travel in the annular bypass to a horizontal plane through the inlet centerline before entering the main duct. The following table presents the dead times calculated in this manner:

Dead time from bypass to the three static-pressure orifices

Configuration	Normal-shock orifice, sec	Bypass orifice, sec	Choke point orifice, sec
Long	0.0108	0.00402	0.00815
Medium	.0108	.00402	.00647
Short	.0108	.00402	.00474

REFERENCES

1. Wilcox, Fred, and Whalen, Paul: Dynamics of a Supersonic Inlet with Adjustable Bypass in Combination with a J34 Turbojet Engine. NACA RM E55L13a, 1956.
2. Hurrell, Herbert G.: Experimental Investigation of Dynamic Relations in a 48-Inch Ram-Jet Engine. NACA RM E56F28, 1957.
3. Hurrell, Herbert G.: Simplified Theory for Dynamic Relation of Ram-jet Pressures and Fuel Flow. NACA RM E57I13, 1957.
4. McGregor, W. K., Russell, D. W., Messick, R. W., and Burns, L. F.: Analysis of Gas Flow Systems for Dynamic Control Purposes. TR-55-11, Arnold Eng. Dev. Center, Apr. 1956. (Contract AF-40(600)-620.)
5. Lubick, Robert J., Chelko, Louis J., and Wallner, Lewis E.: Effect of Inlet-Duct Length in Uniform-Flow Field on Turbojet-Engine Operation. NACA RM E55K15, 1956.
6. Beheim, Milton A., and Englert, Gerald W.: Effect of a J34 Turbojet Engine on Supersonic Diffuser Performance. NACA RM E55I21, 1956.
7. Wilcox, Fred A.: Investigation of a Continuous Normal-Shock Positioning Control for a Translating-Spike Supersonic Inlet in Combination with J34 Turbojet Engine. NACA RM E57G16, 1957.

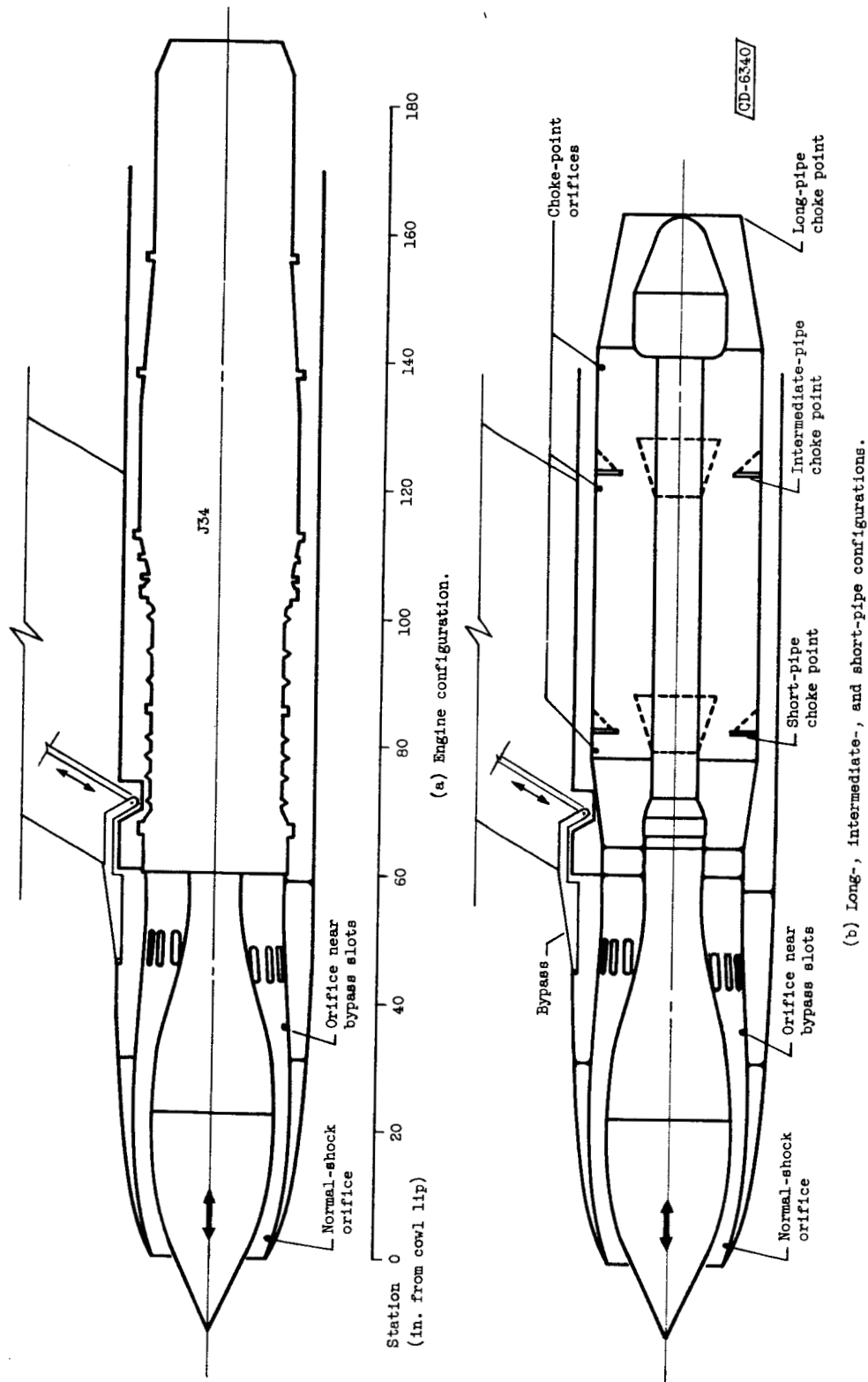


Figure 1. - Test configurations.

0371230 1330

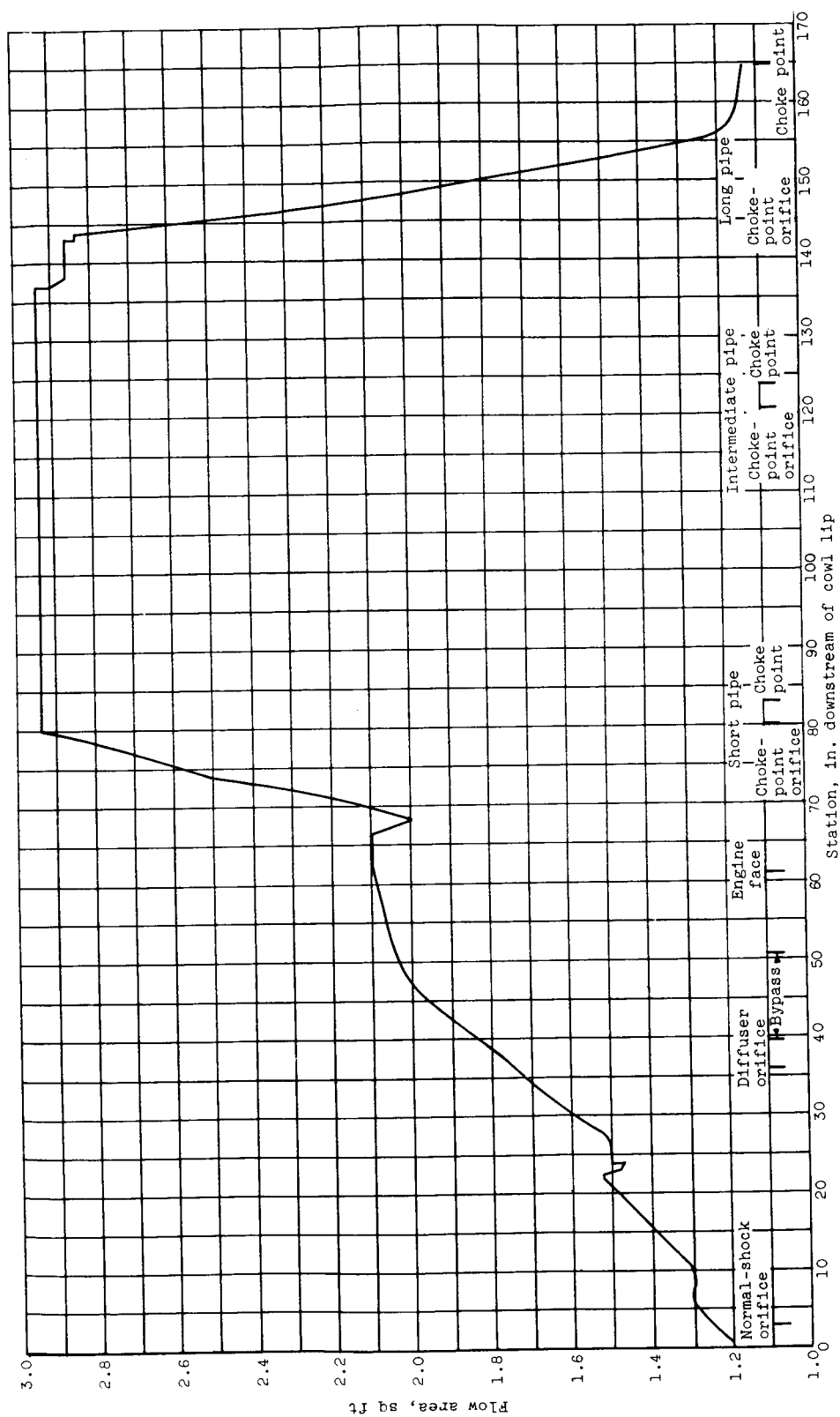


Figure 2. - Inlet and cold-pipe flow area. Spike-position parameter, 45°.

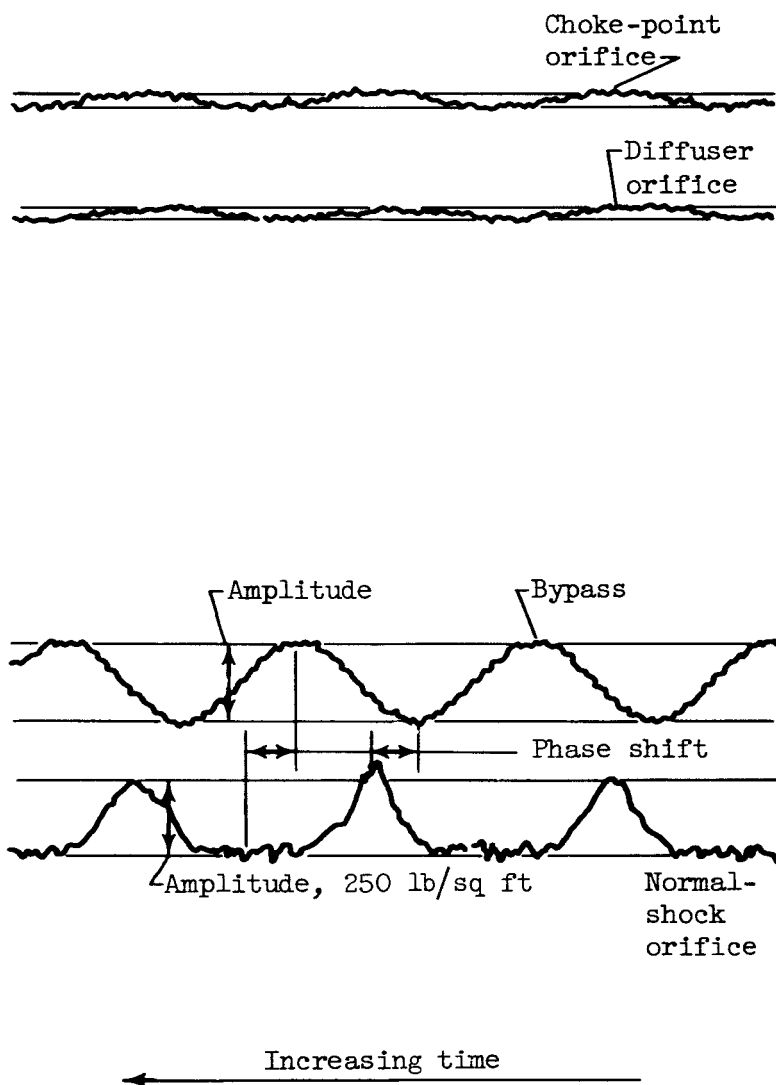


Figure 3. - Typical optical recorder trace.

0371030 1938

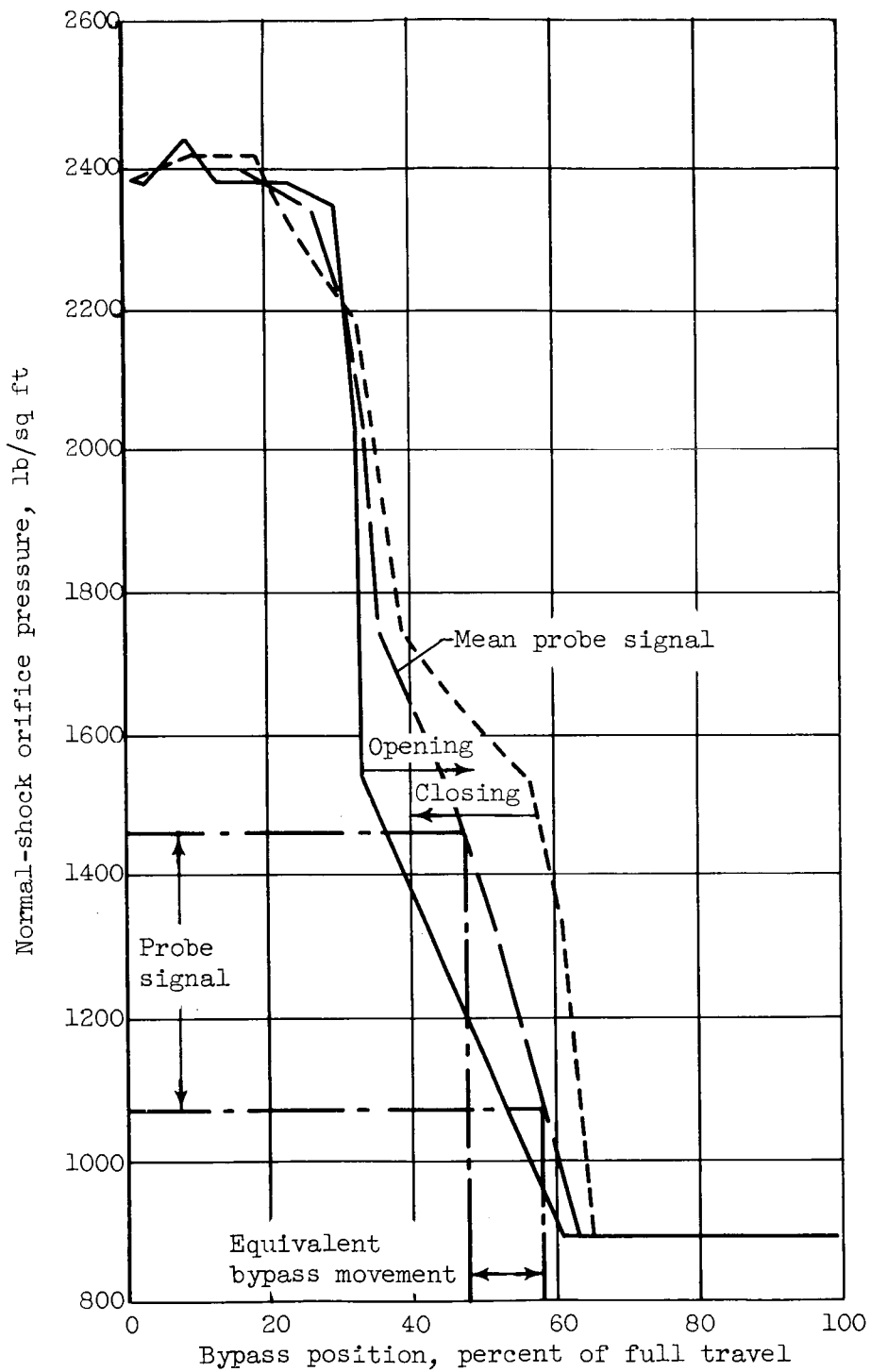
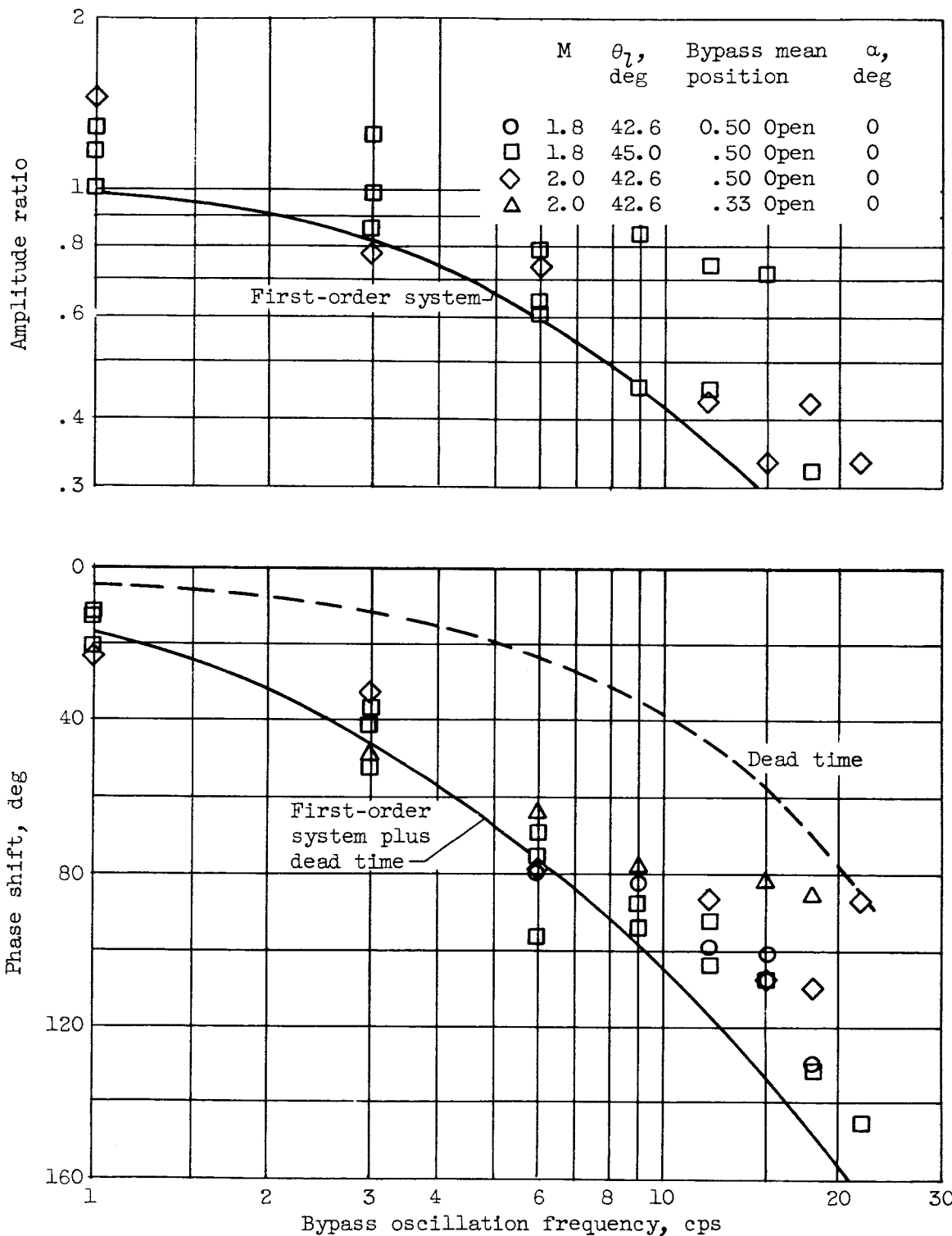


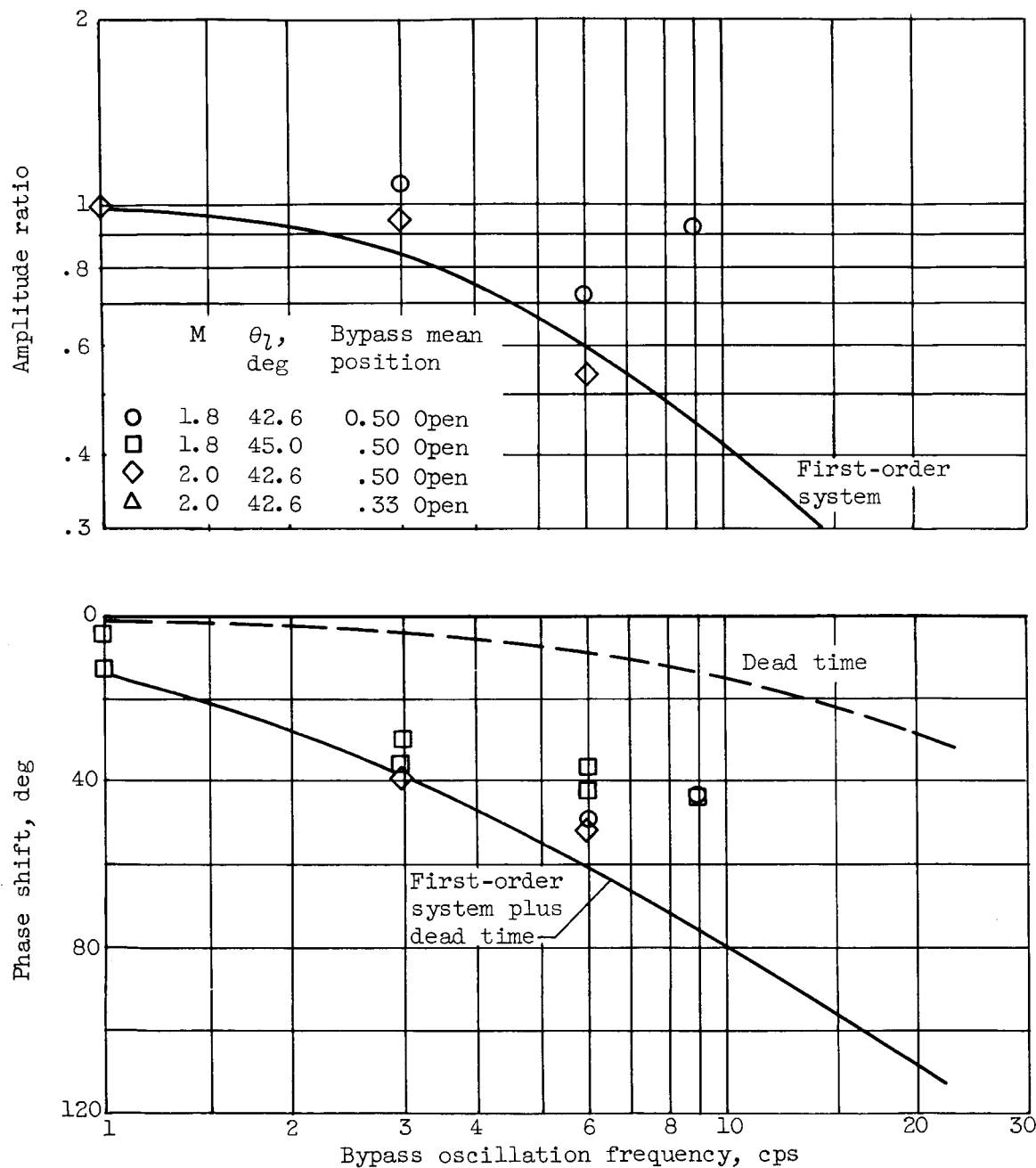
Figure 4. - Pressure variation at normal-shock orifice with bypass movement.



(a) Long-pipe configuration, normal-shock region.

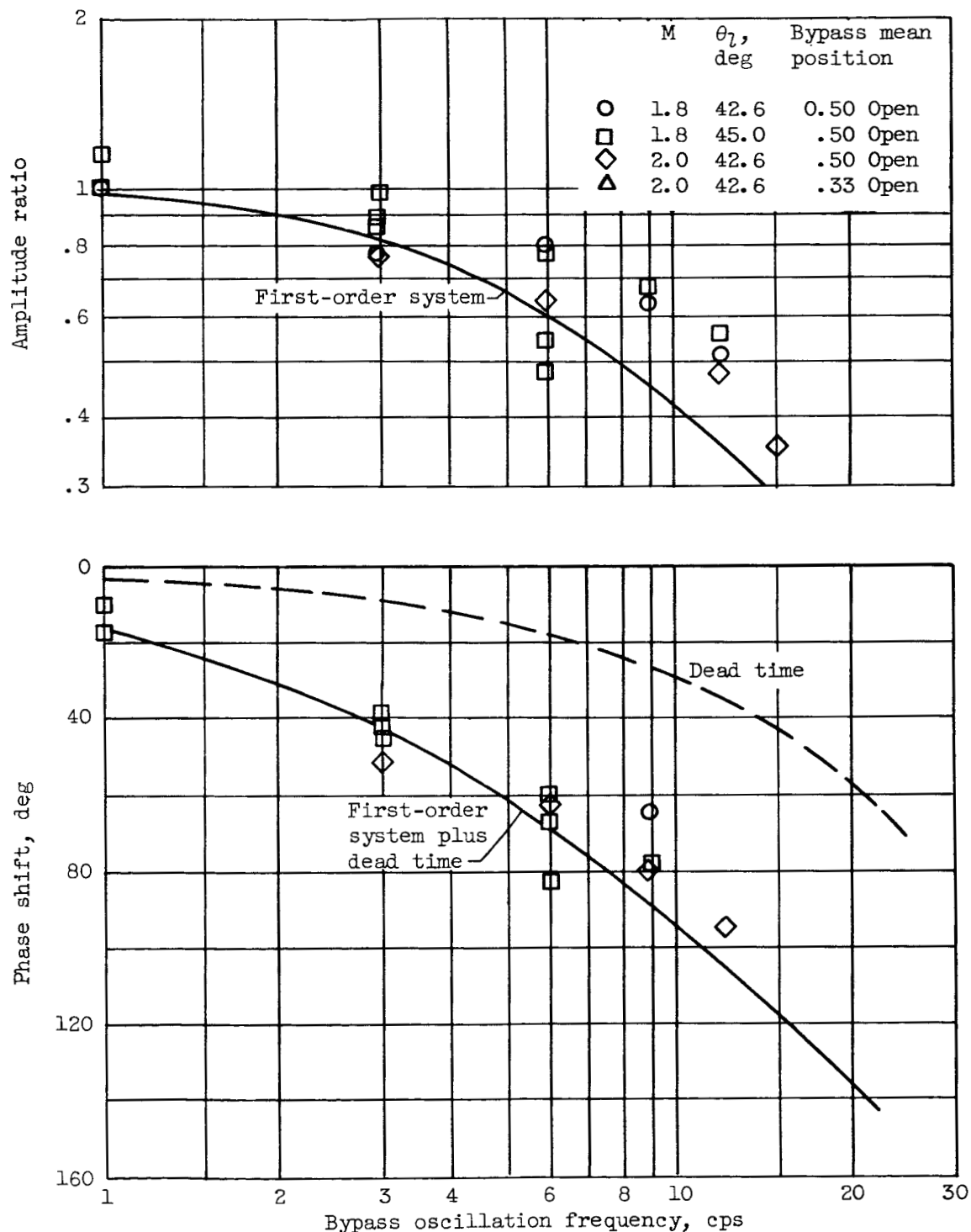
Figure 5. - Dynamic response of static pressures to bypass oscillation.

0371200 1330



(b) Long-pipe configuration, near bypass slots.

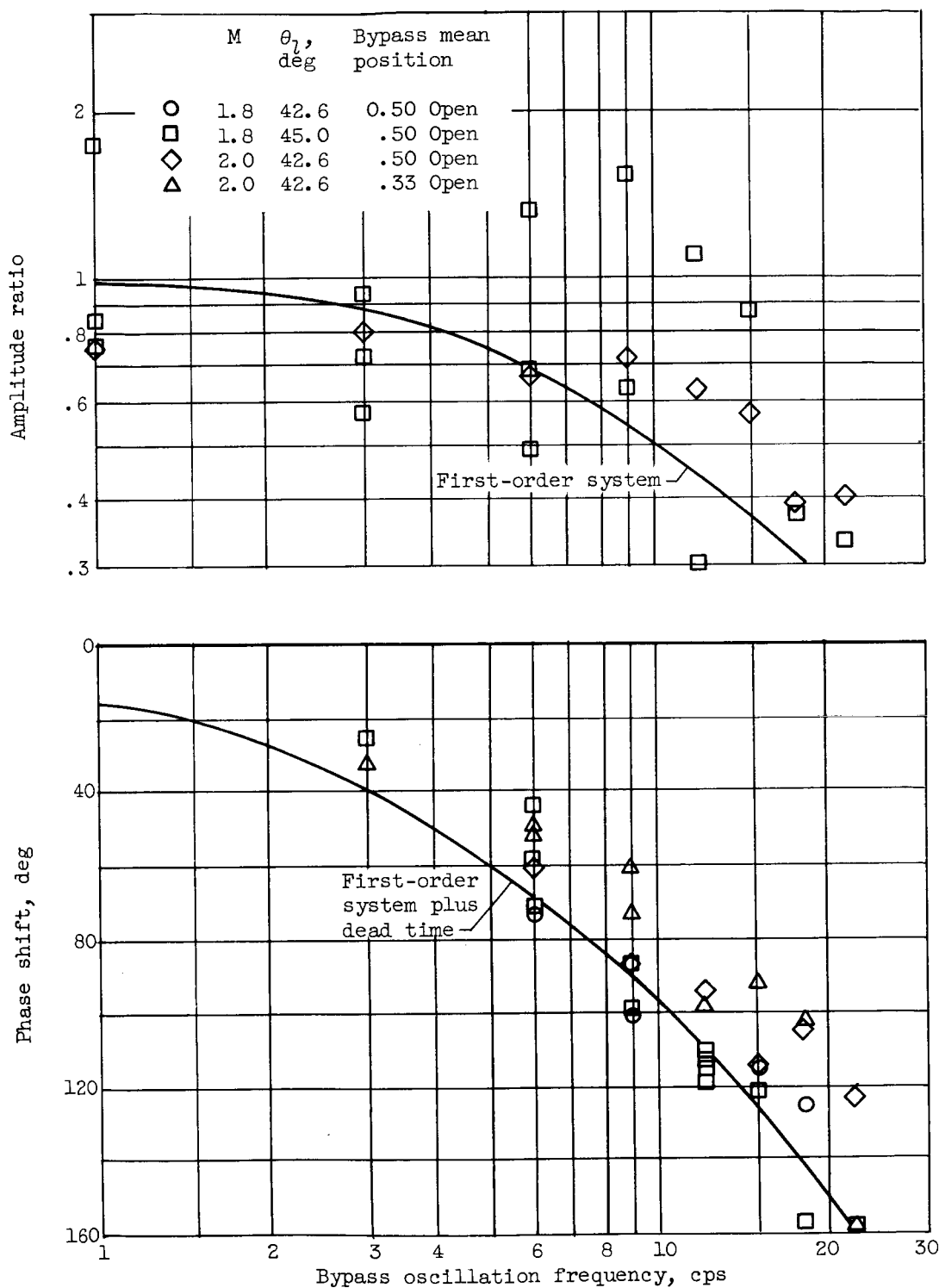
Figure 5. - Continued. Dynamic response of static pressures to bypass oscillation.



(c) Long-pipe configuration, choke point.

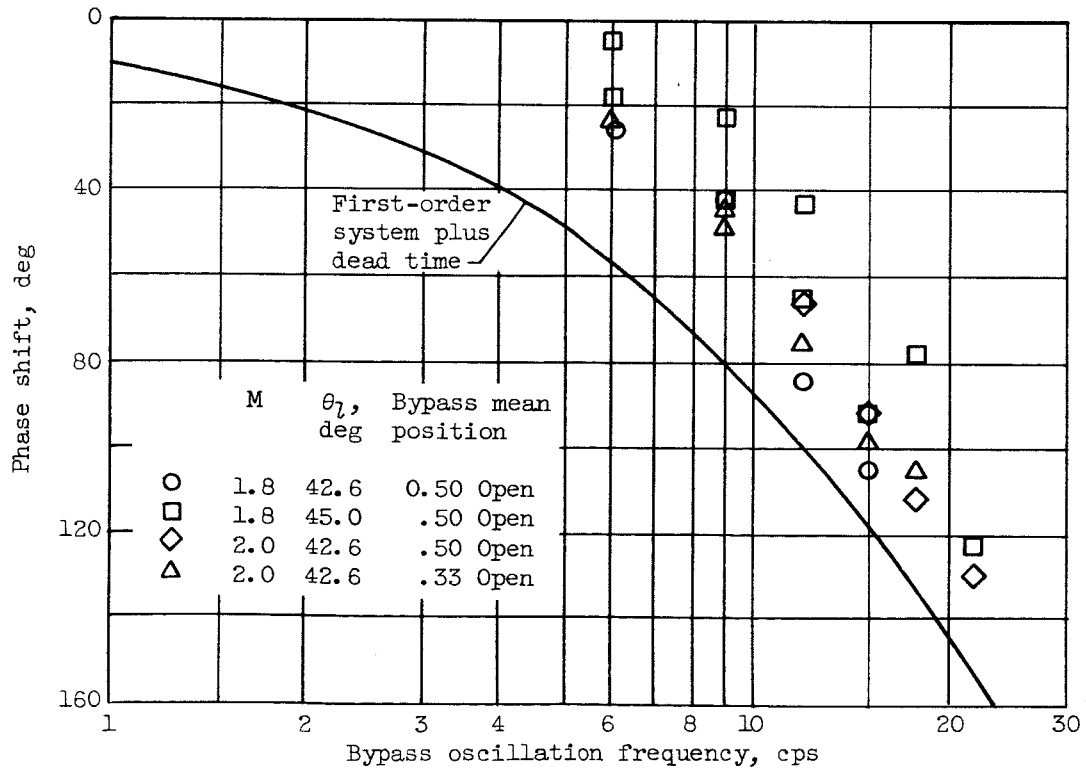
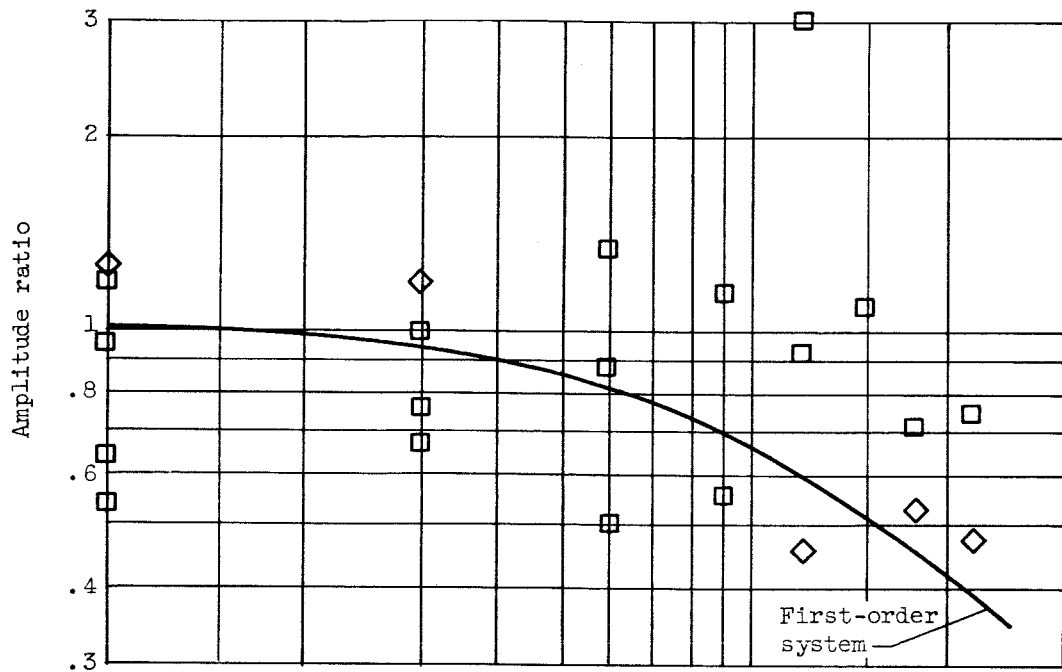
Figure 5. - Continued. Dynamic response of static pressures to bypass oscillation.

03171200 1938



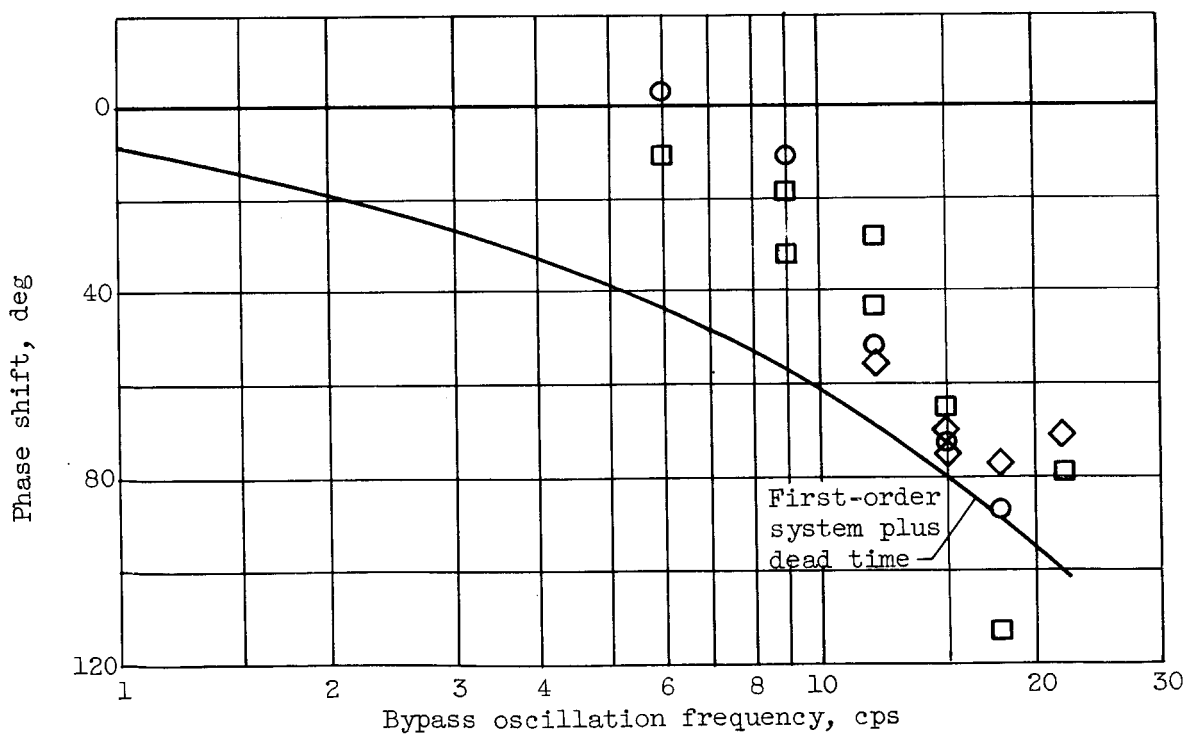
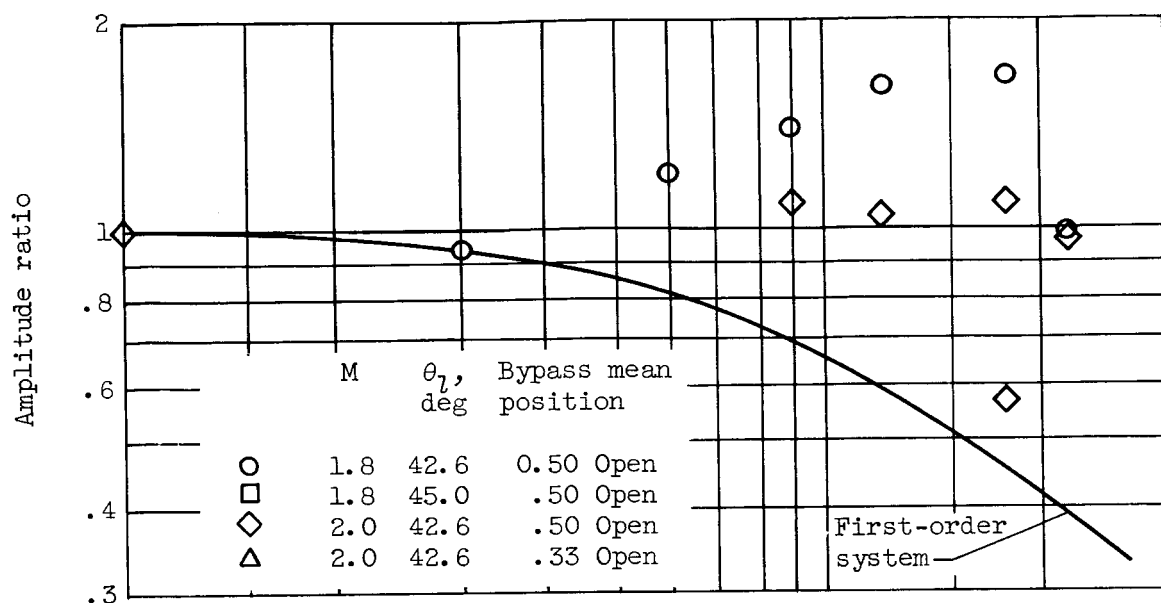
(d) Intermediate-pipe configuration, normal-shock region.

Figure 5. - Continued. Dynamic response of static pressures to bypass oscillation.



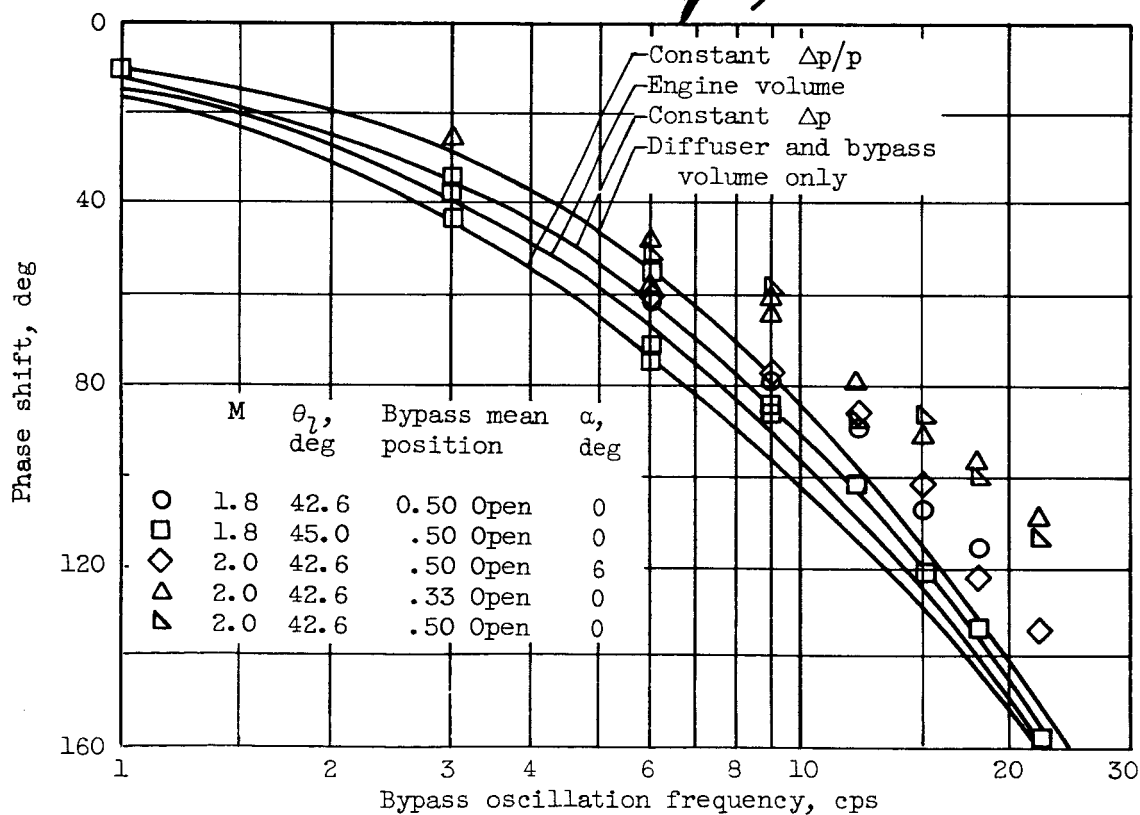
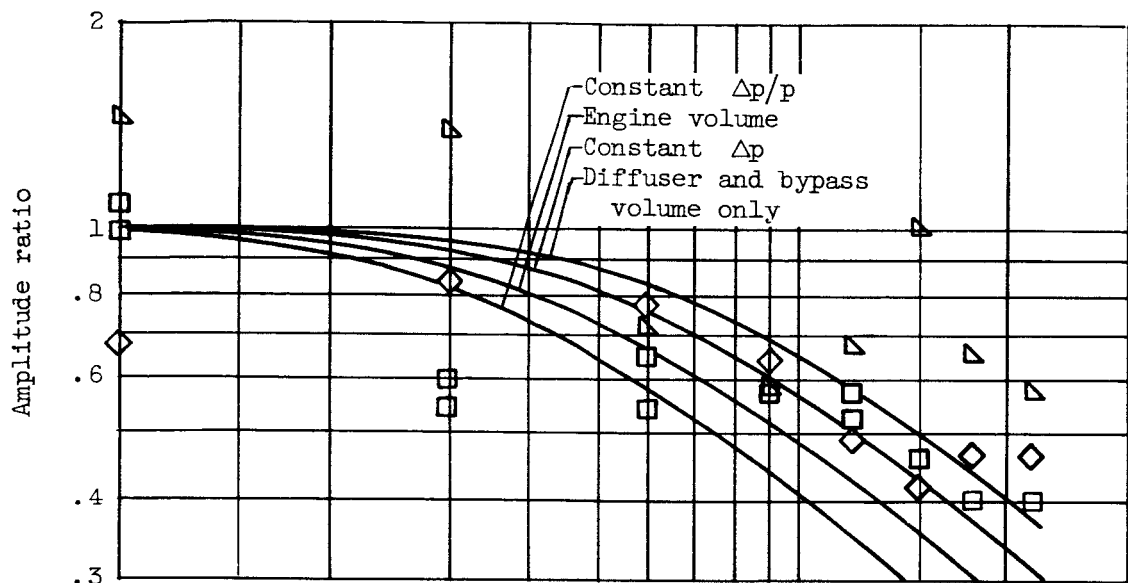
(e) Short-pipe configuration, normal-shock region.

Figure 5. - Continued. Dynamic response of static pressures to bypass oscillation.



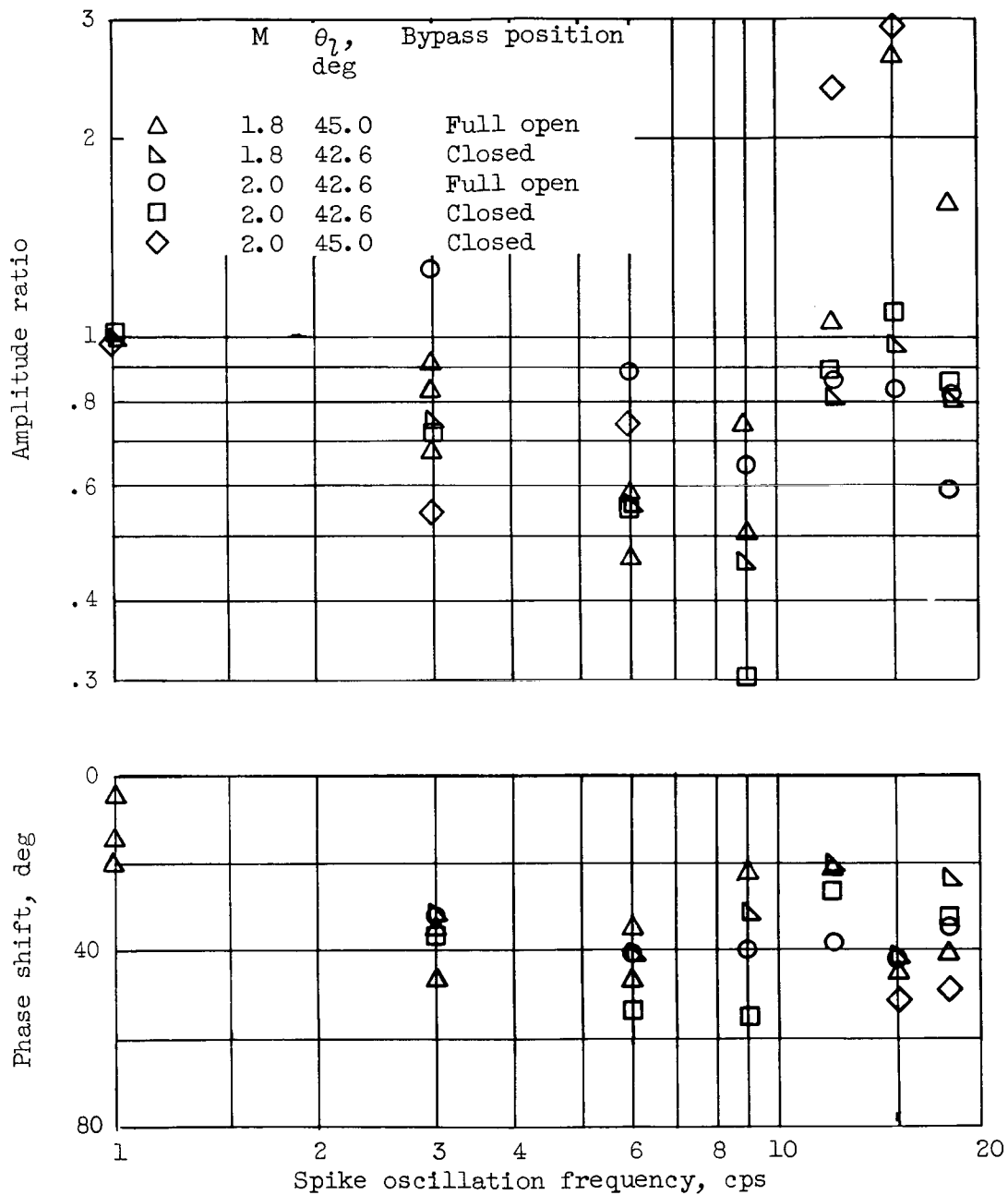
(f) Short-pipe configuration, near bypass slots.

Figure 5. - Continued. Dynamic response of static pressures to bypass oscillation.



(g) Engine configuration, normal-shock region.

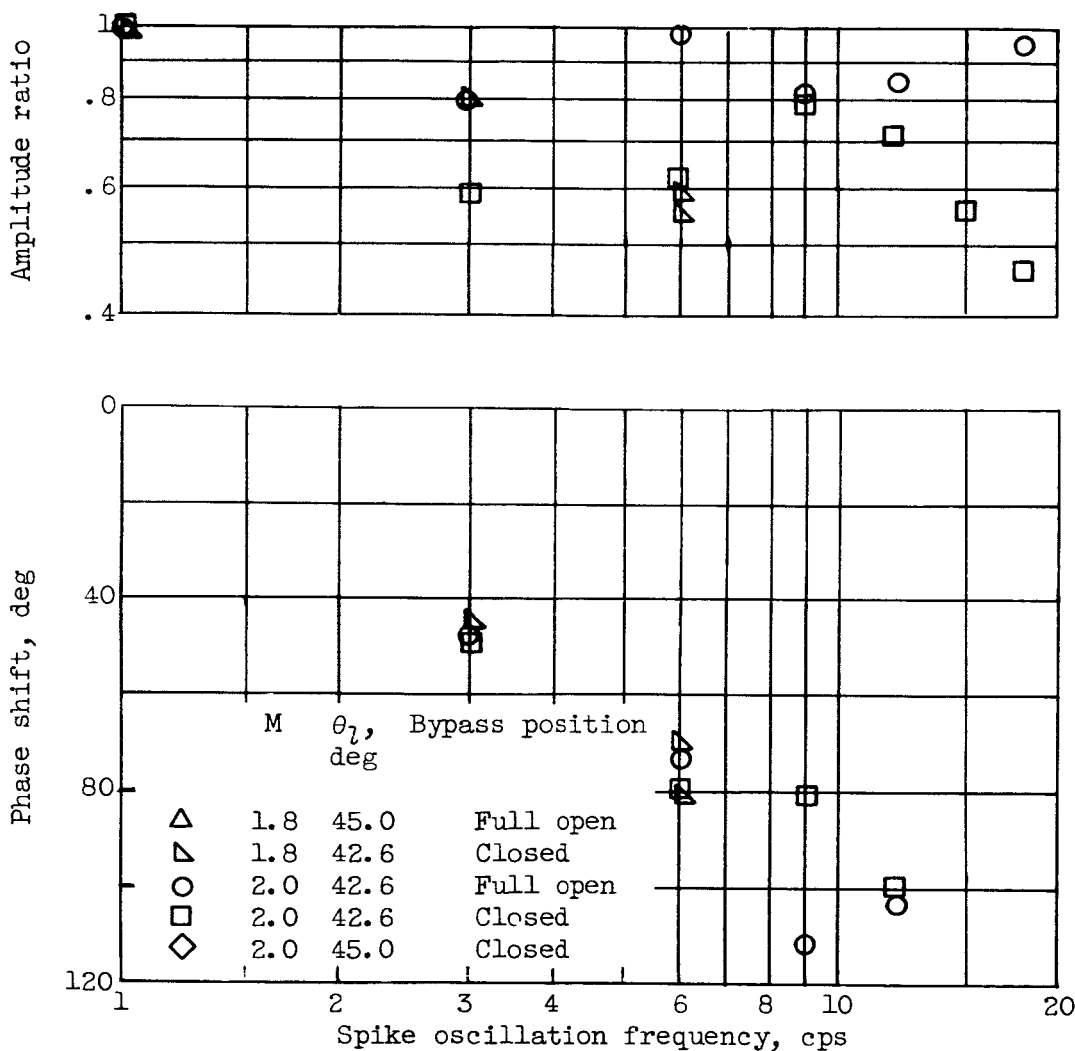
Figure 5. - Concluded. Dynamic response of static pressures to bypass oscillation.



(a) Long-pipe configuration, normal-shock region.

Figure 6. - Dynamic response of static pressures to spike oscillation.

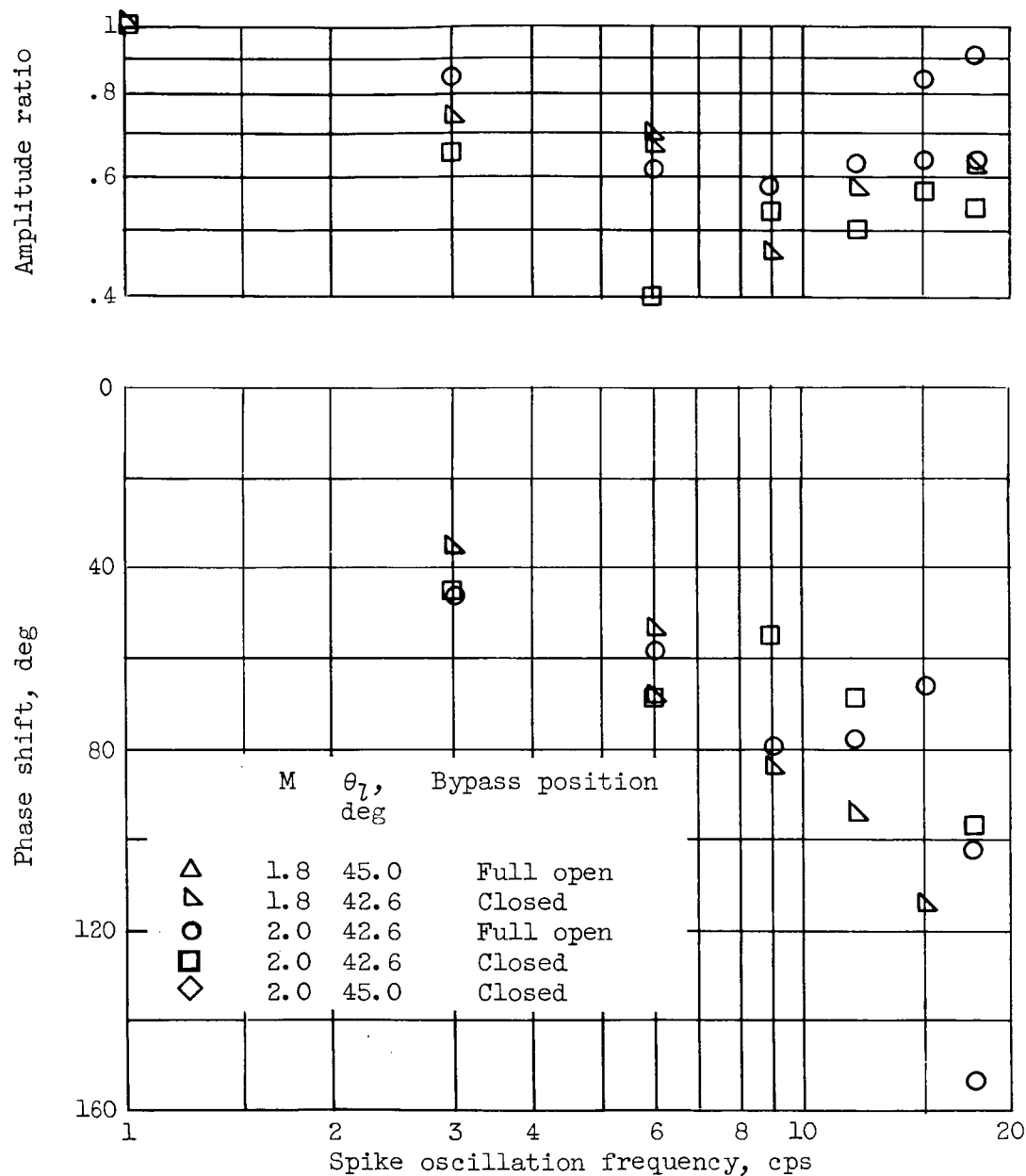
SECRET



(b) Long-pipe configuration, near bypass slots.

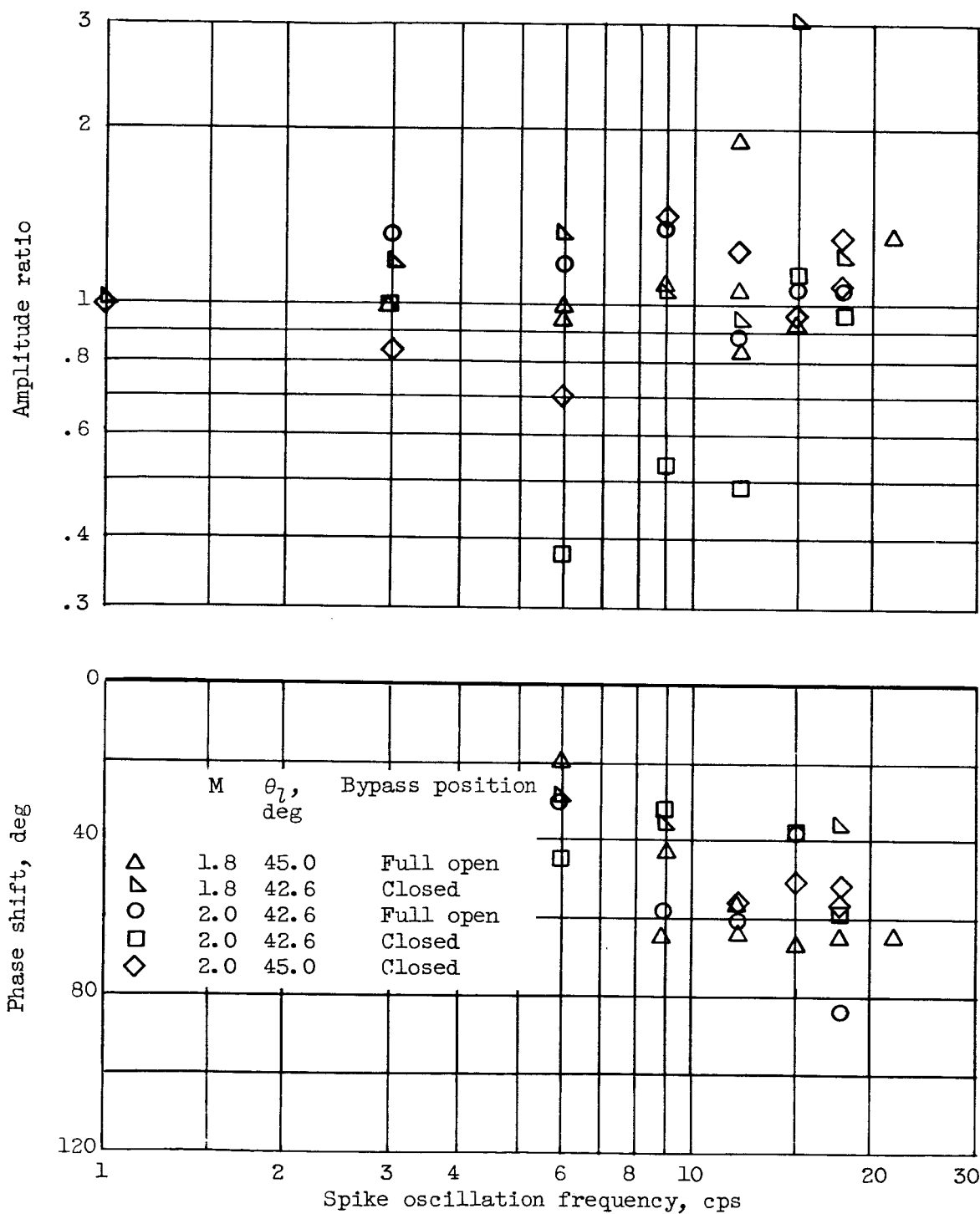
Figure 6. - Continued. Dynamic response of static pressures to spike oscillation.

0317028 030



(c) Long-pipe configuration, near choke point.

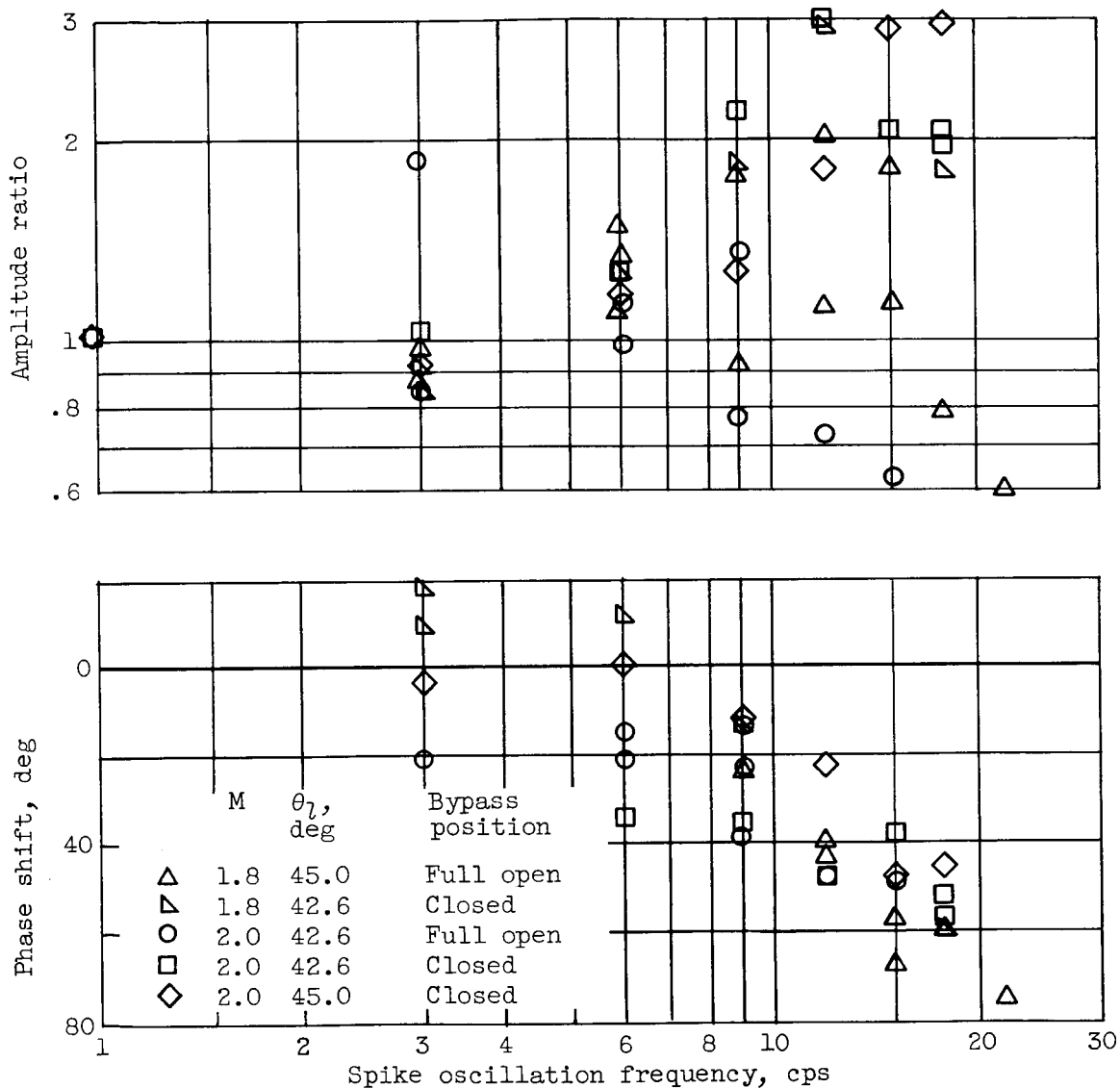
Figure 6. - Continued. Dynamic response of static pressures to spike oscillation.



(d) Intermediate-pipe configuration, normal-shock region.

Figure 6. - Continued. Dynamic response of static pressures to spike oscillation.

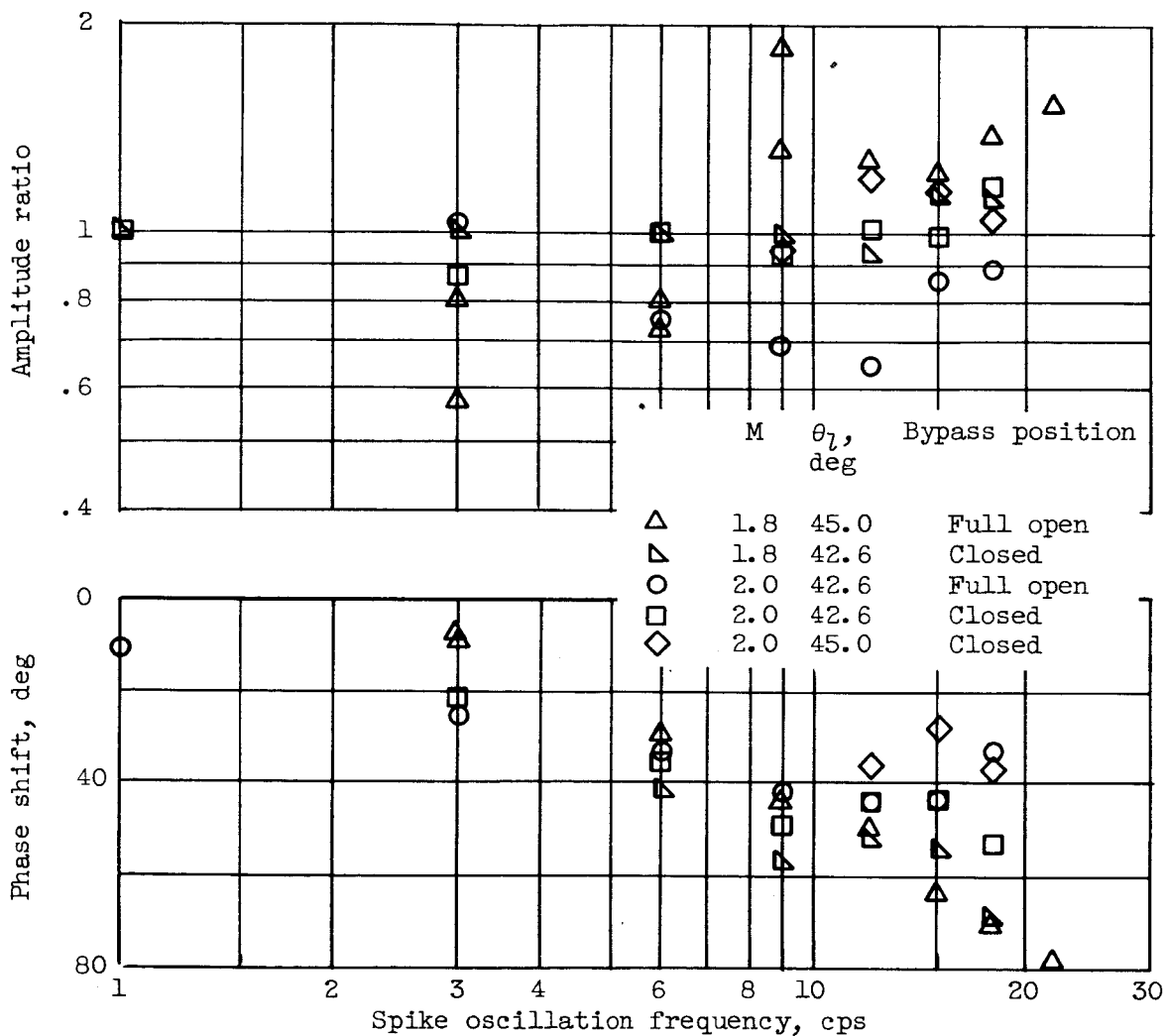
03171220 130



(e) Short-pipe configuration, normal-shock region.

Figure 6. - Continued. Dynamic response of static pressures to spike oscillation.

E-143



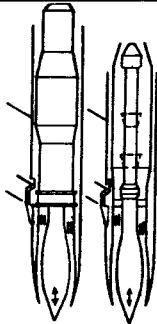
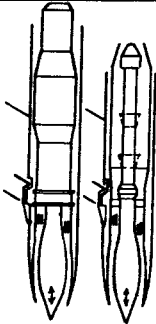
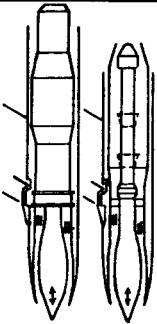
(f) Engine configuration, normal-shock region.

Figure 6. - Concluded. Dynamic response of static pressures to spike oscillation.

NOTES: (1) Reynolds number is based on the diameter of a circle with the same area as that of the capture area of the inlet.

(2) The symbol * denotes the occurrence of buzz.

INLET BIBLIOGRAPHY SHEET

Report and facility	Description			Test parameters				Test data				Performance		Remarks
				Free-stream Mach number	Reynolds number $\times 10^{-6}$	Angle of attack, deg	Angle of yaw, deg	Drag	Inlet flow profile	Discharge-flow profile	Flow picture	Maximum total-pressure recovery	Mass-flow ratio	
CONFID. NASA TM X-10 Lewis 8- by 6-ft Supersonic Wind Tunnel		1	None	2.0 and 1.8	5.3	0°, 6°	0°	No	No	No	No	No	No	Measurement and prediction of dynamic response of static pressure throughout subsonic duct
CONFID. NASA TM X-10 Lewis 8- by 6-ft Supersonic Wind Tunnel														Measurement and prediction of dynamic response of static pressure throughout subsonic duct
CONFID. NASA TM X-10 Lewis 8- by 6-ft Supersonic Wind Tunnel		1	None	2.0 and 1.8	5.3	0°, 6°	0°	No	No	No	No	No	No	Measurement and prediction of dynamic response of static pressure throughout subsonic duct
CONFID. NASA TM X-10 Lewis 8- by 6-ft Supersonic Wind Tunnel														Measurement and prediction of dynamic response of static pressure throughout subsonic duct
CONFID. NASA TM X-10 Lewis 8- by 6-ft Supersonic Wind Tunnel		1	None	2.0 and 1.8	5.3	0°, 6°	0°	No	No	No	No	No	No	Measurement and prediction of dynamic response of static pressure throughout subsonic duct
CONFID. NASA TM X-10 Lewis 8- by 6-ft Supersonic Wind Tunnel														Measurement and prediction of dynamic response of static pressure throughout subsonic duct

Bibliography

These strips are provided for the convenience of the reader and can be removed from this report to compile a bibliography of NASA inlet reports. This page is being added only to inlet reports and is on a trial basis.